

Failure of the conformal-map method for relativistic quantum billiards

Barbara Dietz^{1, 2, *}

¹*Center for Theoretical Physics of Complex Systems,
Institute for Basic Science (IBS), Daejeon 34126, Korea*

²*Basic Science Program, Korea University of Science and Technology (UST), Daejeon 34113, Korea*

(Dated: September 5, 2025)

In [H. Xu *et.al.*, Phys. Rev. Lett. **110**, 064102 (2013)] a numerical method is introduced – an extension of the conformal-map method of [M. Robnik, J. Phys. A: Math. Gen. **17**, 1049 (1984)] for nonrelativistic quantum billiards – for the quantization of relativistic neutrino billiards (NBs) consisting of a massless non-interacting spin-1/2 particle confined to a two-dimensional domain. We demonstrate in this work, that this method does not provide solutions of the associated Weyl (Dirac) equation, nor does it fulfill the boundary conditions imposed on the spinor eigenfunctions to ensure confinement of the particle to the domain of the billiard. We review in detail the wave equation, boundary conditions and quantization of NBs and derivation of relevant equations, to make the proof comprehensible for the general reader. Our results are corroborated with numerical ones for non-relativistic and relativistic quantum billiards whose shapes depend on a parameter, which allows the study of the properties of their eigenstates as the classical dynamics experiences a transition from regular to chaotic dynamics.

I. INTRODUCTION

Billiards have served since the 1980th as a paradigm model for theoretical, numerical and experimental investigations of aspects of quantum chaos [1–3]. In the classical limit they refer to a bounded two-dimensional domain, in which a point particle moves freely and is reflected specularly at the boundary and have the particular property that their dynamics can be controlled by their shape. Nonrelativistic quantum billiards (QBs) are governed by the Schrödinger equation for a free particle which is confined to the billiard domain by imposing on the wave functions the Dirichlet boundary condition (BC) [4–7], and can be realized experimentally with flat microwave cavities [5, 8–13]. In 1987 Berry and Mondragon proposed relativistic neutrino billiards [14] (NBs). These are governed by the Weyl (Dirac) equation for a spin-1/2 particle which is confined to the billiard area by imposing the BC that there is no outward current.

For the study of spectral properties of QBs and NBs generally complete sequences of several 1000th of eigenvalues are needed. Their determination can be intricate and may require sophisticated methods, especially when the classical dynamics is close to integrable implying that the spacings between adjacent eigenvalues may become much smaller than their mean value. Such methods have been developed for nonrelativistic billiards based on the finite-element method [15], which in the mean time has been elaborated considerably, and for high-lying eigenstates one involving the boundary norm [16]. The boundary-integral method (BIM) has been introduced in Ref. [17] for QBs, in [14] for massless NBs and for massive ones in [18, 19]. It originates from the Green theorem, which provides an exact integral equation for the eigenfunctions in the interior of a QB or NB in terms of those

on the boundary, that is, the associated BCs are incorporated. In principle it is applicable to arbitrary shapes and has been applied even to dielectric billiards [20], for which one has to deal with singularities [21, 22]. However, modifications might be needed, e.g., when there are inner corners [23]. In the presence of nearly degenerate eigenvalues one might have to struggle in both cases with missing levels. For that case an expanded BIM has been developed in Refs. [24, 25]. Yet, for NBs, the occurrence of nearly degenerate eigenvalues is considerably less an issue than for nonrelativistic ones, and can generally be removed when they originate from discrete rotational symmetries by separating into the associated symmetry classes [17, 26].

In [27] a conformal-map method (CMM) has been introduced for the quantization of QBs whose shapes are generated from a conformal mapping of the circle, which provides the solutions of the associated Schrödinger equation with high accuracy. The method uses an expansion in terms of the eigenstates of the corresponding circle QB, which complies with the Dirichlet BC along the boundary of the QB by construction. This CMM has been applied to NBs, e.g., in [28–31] to analyze relativistic quantum scars. We will demonstrate in this work, that the CMM does not provide the eigenstates of NBs, although the eigenvalues might be close to the exact ones for sufficiently small deformations of the circular NB.

II. REVIEW OF NEUTRINO BILLIARDS

We consider two-dimensional neutrino billiards (NBs), that were introduced in Ref. [14]. A NB consists of a massless relativistic spin-1/2 particle moving in a bounded two-dimensional region and is described by the Weyl equation [32] for Weyl fermions, which is generally

* bdietzp@gmail.com

referred to as Dirac equation,

$$\hat{\mathbf{H}}_D \psi = c \hat{\boldsymbol{\sigma}} \cdot \hat{\mathbf{p}} \psi = E \psi, \psi = \begin{pmatrix} \psi_1 \\ \psi_2 \end{pmatrix}. \quad (1)$$

Here, $\hat{\mathbf{p}} = -i\hbar \nabla$ is the momentum of the particle, $\hat{\mathbf{H}}_D$ denotes the Dirac Hamilton operator, $\hat{\boldsymbol{\sigma}} = (\hat{\sigma}_x, \hat{\sigma}_y)$, and $\hat{\sigma}_{x,y,z}$ are the Pauli matrices. The energy of the particle is $E = \hbar c k$, where k is the free-space wave vector and c is the velocity of light in vacuum. The particle is confined to the billiard domain by imposing the BC that the outward flux vanishes. Accordingly, the normal component of the local current, that is, of the expectation value of the current operator $\hat{\mathbf{u}} = \nabla_{\mathbf{p}} \hat{\mathbf{H}}_D = c \hat{\boldsymbol{\sigma}}$ is required to vanish along the boundary [33],

$$\mathbf{n} \cdot [\psi^\dagger \nabla_{\mathbf{p}} \hat{\mathbf{H}}_D \psi] = c \mathbf{n} \cdot [\psi^\dagger \hat{\boldsymbol{\sigma}} \psi] = 0. \quad (2)$$

We consider NBs whose domain Ω can be defined in a cartesian coordinate system in polar coordinates, $\mathbf{r} = [x(r, \varphi), y(r, \varphi)]$, or in the complex plane,

$$w(r, \varphi) = x(r, \varphi) + iy(r, \varphi), \varphi \in [0, 2\pi], r \in [0, r_0] \quad (3)$$

with the boundary $\partial\Omega$ at $r = r_0$ denoted as $w(\varphi) \equiv w(r = r_0, \varphi)$. Then, the BC, Eq. (2), reads [14]

$$\psi_2(\varphi) = i\mu B(\varphi) e^{i\alpha(\varphi)} \psi_1(\varphi). \quad (4)$$

Here, $\alpha(\varphi)$ is the angle of the outward-pointing normal vector $\mathbf{n} = [\cos \alpha(\varphi), \sin \alpha(\varphi)]$ at $w(\varphi)$ with respect to the x axis, and $\mu = \pm 1$ determines the rotational direction of the current at the boundary. We use $\mu = 1$ in the following and $B(\varphi) = 1$ in accordance with Ref. [14].

The normal vector \mathbf{n} can be expressed in terms of the derivative $dw(\varphi)/d\varphi = w'(\varphi)$, $e^{i\alpha(\varphi)} = -i \frac{w'(\varphi)}{|w'(\varphi)|}$, yielding the BC

$$\psi_2(\varphi) = \frac{w'(\varphi)}{|w'(\varphi)|} \psi_1(\varphi). \quad (5)$$

Here, we used that for fixed $r = r_0$ we have $w'(z) = -\frac{i}{r_0 e^{i\varphi}} w'(\varphi)$. Note, that $\frac{d\alpha(\varphi)}{d\varphi} = \kappa(\varphi) |w'(\varphi)|$, with $\kappa(\varphi)$ denoting the curvature of the boundary at φ .

We restrict throughout the work to NBs whose shapes are generated by a conformal mapping of the circle defined in terms of polar coordinates $0 \leq r \leq r_0$ and $0 \leq \varphi \leq 2\pi$ by a polynomial in z ,

$$w(z) = x(r, \varphi) + iy(r, \varphi) = \sum_{l \geq 0} c_l z^l, z = re^{i\varphi}, \quad (6)$$

for $r \in [0, r_0]$, $\varphi \in [0, 2\pi]$, $w'(z) \neq 0$. Here, the c_l are real or complex coefficients. For $r < r_0$ and $r = r_0$, $w(z)$ parameterizes the billiard domain Ω and boundary $\partial\Omega$, respectively. The transformation Eq. (3) from (x, y) to $w(z = re^{i\varphi})$ yields for the gradient in the complex plane

$$\frac{\partial}{\partial x} + i \frac{\partial}{\partial y} = \frac{1}{[zw'(z)]^*} \left(r \frac{\partial}{\partial r} + i \frac{\partial}{\partial \varphi} \right), \quad (7)$$

where the star $*$ denotes complex conjugation, leading to the Dirac equation, which consists of coupled equations for the spinor components $\psi_1(r, \varphi)$ and $\psi_2(r, \varphi)$,

$$ik\psi_1(r, \varphi) = \frac{1}{[zw'(z)]} \left(r \frac{\partial}{\partial r} - i \frac{\partial}{\partial \varphi} \right) \psi_2(r, \varphi), \quad (8)$$

$$ik\psi_2(r, \varphi) = \frac{1}{[zw'(z)]^*} \left(r \frac{\partial}{\partial r} + i \frac{\partial}{\partial \varphi} \right) \psi_1(r, \varphi). \quad (9)$$

Applying the differential operator given in Eq. (7) to Eq. (8) and its complex conjugate to Eq. (9) and using that

$$\left(r \frac{\partial}{\partial r} + i \frac{\partial}{\partial \varphi} \right) z = 0, \quad (10)$$

and Eq. (7) gives for each spinor component a separate Schrödinger equation,

$$\Delta_{(r, \varphi)} \psi_j(r, \varphi) = -k^2 |w'(z)|^2 \psi_j(r, \varphi), j = 1, 2 \quad (11)$$

with $\Delta_{(r, \varphi)}$ denoting the Laplace operator in polar coordinates. Yet, when solving these wave equations, one needs to take into account that the components are linked through Eq. (8) or, equivalently, through Eq. (9), and along the boundary in addition through the BC Eq. (5).

Solutions of the Dirac equation (8) and (9) can be written in the coordinate system Eq. (3) in terms of a plane-wave expansion of the form [34],

$$\Phi_1(r, \varphi) = \sum_l a_l(k) i^l J_l(k|w(z)|) e^{il\theta(z)}, \quad (12)$$

where $J_l(x)$ denotes the Bessel function of the first kind, the coefficients $a_l(k)$ are complex or real and independent of (r, φ) and $e^{i\theta(z)} = \frac{w(z)}{|w(z)|}$. Namely, inserting this ansatz into Eqs. (8) and (9) yields with equations (S1), (S2) and (S3) in Sec. A for the second component

$$\Phi_2(r, \varphi) = \sum_l a_l(k) i^{l+1} J_{l+1}(k|w(z)|) e^{i(l+1)\theta(z)}, \quad (13)$$

and

$$\begin{aligned} \Delta_{(r, \varphi)} \Phi_j(r, \varphi) \equiv & \\ -k^2 |w'(z)|^2 \sum_l a_l(k) i^{l-1+j} J_{l-1+j}(k|w(z)|) e^{i(l-1+j)\theta(z)}, \end{aligned} \quad (14)$$

with $j = 1, 2$, implying that both spinor components solve the Schrödinger equation for a free particle Eq. (11). To be an eigenstate of the NB with shape $w(z)$, $\Phi_{1,2}(r, \varphi)$ should fulfill at discrete values of k the BC Eq. (5). Finding such solutions can be a cumbersome task. A very efficient method, which is based on the BIM, is introduced in [14].

In [27] a quantization method has been proposed for the eigenstates of nonrelativistic QBs, whose shapes are given by a $w(z)$ with the properties Eq. (6). These are governed by the nonrelativistic Schrödinger equation Eq. (11) subject to the Dirichlet BC. The ansatz for

the eigenfunctions is given in terms of a linear combination of the orthogonal eigenfunctions of the circular QB. For a circular billiard with radius r_0 the domain is described by Eq. (6) with $w(z) = z$, $|w(z)| = r$, $e^{i\theta(z)} = e^{i\varphi}$, and at the boundary $w(\varphi) = r_0 e^{i\varphi}$ and $e^{i\alpha(\varphi)} = e^{i\varphi}$. The eigenvalues ϵ_n are given as the zeros of the Bessel functions and the eigenfunctions $\psi_n(r, \varphi)$ are given in terms of the Bessel functions,

$$J_n(\epsilon_{n,\nu} r_0) = 0, \psi_{n,\nu}^{e,o}(r, \varphi) = J_{n,\nu}(\epsilon_{n,\nu} r) f_{n,\nu}^{e,o}(\varphi), \quad (15)$$

with $\nu = 1, 2, \dots, n = 1, 2, \dots$, $f_n^e(\varphi) = \cos(n\varphi)$ and $f_n^o(\varphi) = \sin(n\varphi)$ for solutions that are symmetric and antisymmetric with respect to the x axis, respectively. The index ν denotes the ν th zero of $J_n(\epsilon_{n,\nu} r_0)$ for a given index n . The ansatz used in [27, 35] for the solutions of the Schrödinger equation Eq. (11) with Dirichlet BCs along the boundary $w(\varphi)$ reads

$$\psi(r, \varphi) = \sum_{n=-\infty}^{\infty} \sum_{\nu=1}^{\infty} \frac{c_{n,\nu}(k) N_{n,\nu}}{\epsilon_{n,\nu}} J_{|n|,\nu}(\epsilon_{n,\nu} r) e^{in\varphi}, \quad (16)$$

with $N_{n,\nu}^{-1} = \sqrt{\pi} |J'_{n,\nu}|$, $c_{n,\nu}$ denoting the expansion coefficients and $\epsilon_{n,\nu} = \epsilon_{-n,\nu}$. These wave functions fulfill the Dirichlet BCs by construction. The eigenvalues and associated eigenstates are obtained by solving the eigenvalue problem

$$\hat{\mathcal{M}}\mathbf{c} = \frac{1}{k^2} \mathbf{c}, \quad (17)$$

with matrix elements $\mathcal{N}_{n\nu m\mu} \hat{\mathcal{M}}_{n\nu m\mu}$ given by

$$\int_0^{r_0} r dr \int_0^{2\pi} d\varphi |w'(z)|^2 e^{i(n-m)\varphi} J_{|n|,\nu}(\epsilon_{n,\nu} r) J_{|m|,\nu}(\epsilon_{m,\mu} r), \quad (18)$$

where $\mathcal{N}_{n\nu m\mu}^{-1} = \frac{N_{n,\nu} N_{m,\mu}}{\epsilon_{n,\nu} \epsilon_{m,\mu}}$. In Sec. IV we demonstrate the efficiency of this method for the Africa QB [35].

III. THE FLAWS OF THE CMM FOR NEUTRINO BILLIARDS

In analogy to the quantization procedure [27, 35], in Ref. [28] a method was proposed for the computation of the eigenstates of NBs on the basis on those of a circular NB. The eigenvalues and eigenfunctions of the circular NB are obtained by imposing the BC Eq. (5) on the ansatz Eq. (12) with the second component given in Eq. (13), leading to the quantization condition [14]

$$J_{m+1}(\kappa_{m,\mu}) = J_m(\kappa_{m,\mu}), \quad (19)$$

where μ counts the number of eigenstates below $\kappa_{m,\mu}$ for a given total angular momentum $m + \frac{1}{2}$, that is, the $\kappa_{m,\mu}$ are sorted as $\kappa_{m,1} \leq \kappa_{m,2} \leq \dots$. The associated eigenfunctions read

$$\begin{aligned} \Phi_{1m,\mu}(r, \varphi) &= \mathcal{N}_{m,\mu} i^m J_m(\kappa_{m,\mu} r) e^{im\varphi}, \\ \Phi_{2m,\mu}(r, \varphi) &= \mathcal{N}_{m,\mu} i^{m+1} J_{m+1}(\kappa_{m,\mu} r) e^{i(m+1)\varphi}. \end{aligned} \quad (20)$$

The spinor eigenfunctions

$$\Phi_{m,\mu}(r, \varphi) = \begin{pmatrix} \Phi_{1m,\mu}(r, \varphi) \\ \Phi_{2m,\mu}(r, \varphi) \end{pmatrix} \quad (21)$$

are orthogonal to each other [14] [cf. Sec. A],

$$\int_0^{r_0} r dr \int_0^{2\pi} d\varphi \Phi_{m,\mu}(r, \varphi) \cdot \Phi_{n,\nu}(r, \varphi) = \delta_{n,m} \delta_{\nu,\mu}. \quad (22)$$

In analogy to Ref. [27] for the CMM the ansatz for the first spinor component consists of a superposition of the eigenfunctions of the circular NB,

$$\begin{aligned} \psi_1(r, \varphi) &= \\ \sum_{n=-\infty}^{\infty} \sum_{\nu=1}^{\infty} a_{n,\nu}(k) i^n J_n(r \kappa_{n,\nu}) e^{in\varphi} &= \sum_j a_j(k) \Phi_{1j}(r, \varphi), \end{aligned} \quad (23)$$

where the index j counts the number of eigenvalues below $\kappa_{l(j),\lambda(j)}$, that is, these are sorted by size, $\kappa_{l(1),\lambda(1)} \leq \kappa_{l(2),\lambda(2)} \leq \dots$. Note, that for circular NBs we have $\kappa_{n,\nu} \neq \kappa_{-n,\nu}$ [14].

The ansatz for the second component, $\psi_2(r, \varphi)$ is obtained by inserting $\psi_1(r, \varphi)$ into the Dirac equation (9), from which the associated Schrödinger equations for the two spinor components, that are solved within the CMM, originate, yielding

$$\begin{aligned} [w'(z)]^* \psi_2(r, \varphi) &= \\ \sum_{n,\nu} b_{n,\nu}(k) i^{n+1} J_{n+1}(r \kappa_{n,\nu}) e^{i(n+1)\varphi} &= \sum_j b_j(k) \Phi_{2j}(r, \varphi), \\ b_{n,\nu}(k) &= \frac{\kappa_{n,\nu}}{k} a_{n,\nu}(k). \end{aligned} \quad (24)$$

Hence, for $k \neq \kappa_{n,\nu}$ and $[w'(z)]^* \neq 1$, that is, for shapes different from a circle we have $\frac{1}{[w'(z)]^*} b_{n,\nu} \neq a_{n,\nu}$, in contrast to the assumptions of [28]. Inserting this result into Eq. (8) yields for $\psi_1(r, \varphi)$ the Schrödinger equation

$$\begin{aligned} \sum_{n,\nu} a_{n,\nu}(k) \kappa_{n,\nu}^2 i^n J_n(\kappa_{n,\nu} r) e^{in\varphi} &= \\ k^2 |w'(z)|^2 \sum_{n,\nu} a_{n,\nu}(k) i^n J_n(\kappa_{n,\nu} r) e^{in\varphi}. \end{aligned} \quad (25)$$

Similarly, inserting Eq. (24) into Eq. (11) for $i = 2$ gives

$$\begin{aligned} r^2 \Delta_{(r,\varphi)} \psi_2(r, \varphi) &= \\ \left(r \frac{\partial}{\partial r} + i \frac{\partial}{\partial \varphi} \right) \left[\frac{iz}{k[w'(z)]^*} \sum_{n,\nu} a_{n,\nu}(k) \kappa_{n,\nu}^2 i^n J_n(r \kappa_{n,\nu}) e^{in\varphi} \right]. \end{aligned} \quad (26)$$

Assuming that the k value is chosen such that the condition Eq. (25) holds to replace the sum over n, ν by the right-hand side of this equation, yields

$$\begin{aligned} \sum_{n,\nu} b_{n,\nu}(k) \kappa_{n,\nu}^2 i^{n+1} J_{n+1}(\kappa_{n,\nu} r) e^{i(n+1)\varphi} &= \\ k^2 |w'(z)|^2 \sum_{n,\nu} b_{n,\nu}(k) i^{n+1} J_{n+1}(\kappa_{n,\nu} r) e^{i(n+1)\varphi} + \delta, \end{aligned} \quad (27)$$

with $\delta = 0$. Yet, when this equation and Eq. (25) do not have solutions at the same values of k , then an additional term

$$\delta = 2ikw'(z)[w''(z)]^*\psi_1(r, \varphi) \quad (28)$$

appears in Eq. (27). Note, that these equations are no identities, but conditional equations for the eigenstates of the associated NB.

Defining in analogy to the nonrelativistic case, Eq. (18), matrices $\hat{\mathcal{K}}_1, \hat{\mathcal{K}}_2, \hat{\mathcal{J}}_1$ and $\hat{\mathcal{J}}_2$, [cf. Eq. (S11) in Sec. A], Eqs. (25) and (27) can be written as

$$[\hat{\mathcal{K}}_1 - k^2 \hat{\mathcal{J}}_1] \mathbf{a} = 0, \quad (29)$$

$$[\hat{\mathcal{K}}_2 - k^2 \hat{\mathcal{J}}_2] \mathbf{b} = 0. \quad (30)$$

They have solutions only for discrete values of $k = \tilde{k}_j$, because the matrices $\hat{\mathcal{K}}_1, \hat{\mathcal{K}}_2, \hat{\mathcal{J}}_1, \hat{\mathcal{J}}_2$ do not depend on k .

In [28] \mathbf{b} entering Eq. (24) is set equal to \mathbf{a} in Eq. (23), and the eigenstates $[\mathbf{a}_j(\tilde{k}_j), \tilde{k}_j]$ of the sum of Eqs. (29) and (30), $[(\hat{\mathcal{K}}_1 + \hat{\mathcal{K}}_2) - \tilde{k}_j^2 (\hat{\mathcal{J}}_1 + \hat{\mathcal{J}}_2)] \mathbf{a}_j = 0$, are determined using the orthogonality Eq. (22),

$$\hat{\mathcal{J}} - \frac{\hat{\kappa}^2}{k^2} = \hat{0}, \quad \hat{\mathcal{J}}_{jj'} = \left(\mathcal{M}_a^T [\hat{\mathcal{J}}_1 + \hat{\mathcal{J}}_2] \mathcal{M}_a \right)_{jj'}, \quad (31)$$

$$\hat{\kappa}_{jj'}^2 = \left(\mathcal{M}_a^T [\hat{\mathcal{K}}_1 + \hat{\mathcal{K}}_2] \mathcal{M}_a \right)_{jj'} = \kappa_j^2 \delta_{jj'},$$

where the column vectors of the matrix \mathcal{M}_a are the eigenvectors \mathbf{a}_j corresponding to the eigenvalues $\tilde{k}_j, j = 1, \dots, N$ and the dimension N equals the number of eigenstates of the circular NB, $\kappa_1 \leq \kappa_2 \leq \dots \leq \kappa_N$, taken into account. Yet, for $\mathbf{b} = \mathbf{a}$ the ansatz for the spinor functions with components Eq. (23) and Eq. (24) is no solution of the Dirac equation (8) with (9). In fact, Eqs. (29), (30) for the spinor components and (31) do not have common solutions and the additional term δ in Eq. (26) is nonzero, except for constant $w'(z)$, that is, for circular shapes. The reason for this deficiency is that, as mentioned above, Eqs. (25) and (27) are no identities, as in the case of the ansatz Eq. (12) with Eq. (13), but conditional equations.

The correct strategy to solve the Dirac equation (8) with (9) using the ansatz Eq. (23), would be to solve the generalized eigenvalue problem Eq. (29) for the first component, because for $\mathbf{a} \neq \mathbf{b}$ the orthogonality of the eigenstates of the circular NB cannot be employed. Then the second component would be obtained from Eq. (24). Again, Eq. (29) has solutions only for discrete values of k , since the matrices $\hat{\mathcal{J}}_i, \hat{\mathcal{K}}_i, i = 1, 2$ are assumed to be independent of k . However, like for the case $\mathbf{a} = \mathbf{b}$ these differ from those of Eq. (30) for non-circular shapes and $\delta \neq 0$ in Eq. (26); cf. Sec. IV and Sec. IV A

By construction, the solutions of Eq. (31) ($\tilde{k}_j, \psi_j(r, \varphi)$) fulfill the BC for circular NBs, $\psi_{1j}(r_0, \varphi) =$

$-ie^{-i\varphi} \psi_{2j}(r_0, \varphi)$, that is,

$$\psi_{1j}(r_0, \varphi) = i^{-1} e^{-i\varphi} \sum_{n, \nu} a_{n, \nu}(\tilde{k}_j) i^{n+1} J_{n+1}(r_0 \kappa_{n, \nu}) e^{i(n+1)\varphi}. \quad (32)$$

Yet, they fail to comply with the BC for NBs, Eq. (5),

$$\psi_{1j}(r_0, \varphi) \neq \frac{1}{|w'(\varphi)|} \sum_{n, \nu} b_{n, \nu}(\tilde{k}_j) i^{n+1} J_{n+1}(r_0 \kappa_{n, \nu}) e^{i(n+1)\varphi}, \quad (33)$$

also when using the correct ansatz Eq. (23) with Eq. (24) for the solutions of the Dirac equation (8) with (9). Indeed, the right-hand sides of equations (32) and (33) are only equal, that is, the BC Eq. (5) only holds for $w'(\varphi) = ie^{i\varphi}, \tilde{k}_j = \kappa_{n, \nu}$, implying that the outgoing flux

$$\mathbf{n} \cdot [\psi^\dagger \hat{\sigma} \psi] = \cos[\alpha(\varphi)] \text{Re}[\psi_1^* \psi_2] + \sin[\alpha(\varphi)] \text{Im}[\psi_1^* \psi_2] \equiv \sin[\alpha(\varphi) - \varphi] |\psi_1(\varphi)|^2, \quad (34)$$

is nonvanishing for non-circular shapes and proportional to the size of the intensity of the wave function $\psi_1(\varphi)$ along the boundary.

The impact of the boundary wave functions $\psi_1(\varphi)$ and $\psi_2(\varphi)$ remains non-negligible in the semiclassical limit $k \rightarrow \infty$ [18]. This can be deduced from the feature of the trace formula, which is the semiclassical approximation for the spectral density in terms of a sum over periodic orbits of the classical billiard of corresponding shape [36]. The difference between the trace formulas for QBs and NBs is, that in the latter contributions of periodic orbits with an odd number of reflections at the boundary are missing, because the contributions from the spinor components of its eigenfunctions cancel each other [14, 18, 37, 38], which would not be possible if they vanished along the boundary like for QBs. Note, that this feature of the trace formula is not a characteristic of relativistic QBs, but it is also observed in non-relativistic systems subject to a vectorial wave equation [39, 40].

Still, the fluctuation properties of the eigenvalues obtained from each of the equations (29), (30) and (31) are expected to be close to those of the NB. Namely, like the eigenfunctions of the circular NB, those of these equations are complex, that is they are not invariant under time-reversal. Furthermore, the potential $|w'(z)|^2$ induces the same chaoticity as for the CMM for nonrelativistic QBs. Accordingly, the spectral properties may not be used as a criterion to prove or disprove the applicability of the CMM for NBs. To illustrate in the Secs. IV and IV A numerically for a few examples the failure of the CMM for NBs, we consider the Weyl formula for the smooth part of the integrated spectral density, which differs for NBs and QBs [14, 32], and demonstrate that that for QBs applies for CMM, whereas for the eigenvalues obtained from BIM excellent agreement with that for NBs is found. Furthermore we compute differences between the eigenvalues obtained with equations (29), (30), and from the BIM and Eq. (31), respectively, and compare wave functions obtained with BIM and CMM.

We conclude that the method proposed in [28, 29] for the determination of the eigenstates of NBs is only applicable to the circular NB, that is for the trivial case. Otherwise, it does not provide reliable solutions, because these do not comply with the Dirac equation and BCs for neutrino billiards. It is stated in these works that the solutions of the CMM fulfill the BC Eq. (5). Yet, for this the second spinor component $\psi_2(r, \varphi)$, Eq. (24) needs to be multiplied with a φ -dependent factor, which can be read off Eqs. (32) and (33). However then, even when using the correct ansatz for the spinor components, Eq. (23) and Eq. (24), the Dirac equation is not fulfilled since application of the operator Eq. (7) to this factor is nonvanishing. This reflects the fact, that it is not sufficient to solve the Schrödinger equation for the spinor components, as demonstrated, e.g., for the ellipse NB in [41].

In Ref. [30] the authors apply the same method to massive NBs with mass $m_0 \neq 0$. We demonstrate in Ref. [18], that the corresponding Dirac equation can be brought to the same form as in (8) and (9) with modified BCs that comply with the ultrarelativistic limit $m_0 \rightarrow 0$ for massless NBs and the nonrelativistic limit, $\frac{m_0 c}{\hbar k} \rightarrow \infty$. Starting from this Dirac equation with modified BCs and proceeding as above, it can be shown, that the method of [30] does not provide the eigenstates of NBs with non-circular shapes.

In the Secs. IV and IV A we provide examples, which show that the eigenvalues obtained from Eq. (31) can be close to those of the corresponding NB, for shapes with nearly constant curvature except in small parts of the boundary, however not the eigenfunctions. So as long as one is not interested in the eigenfunctions and their phases, and the shape is close to that of a circle, it can serve as an approximate method to determine a few 1000th of eigenvalues. On the other hand, the BIM introduced in Ref. [14] for the ultrarelativistic case and its extension to massive NBs [18, 42] yields at least that many eigenvalues with low numerical effort – especially for the NBs under consideration – and also the associated eigenfunctions with high precision. Thus, there is no reason to use a method, which has been proven to be erroneous and thus provides unreliable eigenstates. The flaws of the CMM unveiled in this work, in fact explain the discrepancies between the solutions of the CMM and expected results observed, e.g. in Refs. [30, 31].

IV. NUMERICAL ANALYSIS OF THE CMM FOR BILLIARDS FROM THE FAMILY OF THE AFRICA BILLIARD FOR WHICH THE EIGENVALUES ARE CLOSE TO THOSE OF THE NB

We compare results obtained with the CMM and the BIM, respectively, for a family of billiards with shapes given as [14, 35]

$$w^{AF}(z; \alpha) = \frac{z + \alpha z^2 + \alpha e^{i\pi/3} z^3}{\sqrt{1 + 5\alpha^2}}. \quad (35)$$

For $\alpha = 0$ the shape is circular, whereas with increasing α the classical dynamics undergoes a transition from regular via mixed regular-chaotic to chaotic. We computed eigenstates for several values of $\alpha \leq 0.2$. In the inset of the left part of Fig. 1 shapes are shown for $\alpha = 0$ (black), and for the cases considered, $\alpha = 0.1$ (blue), $\alpha = 0.125$ (red) and $\alpha = 0.2$ (green). For the latter one, known as 'Africa billiard', the dynamics is chaotic. Furthermore, the angle $\alpha(s)$ of the normal vector with respect to the x-axis and the curvature $\kappa(s)$ are exhibited as function of the arclength parameter. The angle $\alpha(s)$ varies nearly linearly with s and the curvature is close to unity, i.e. to that of a circle of radius unity, except in the regions around the two bulges.

To verify correctness of the codes used to solve Eqs. (29), (30) and (31), we first applied the CMM Eq. (17) with Eq. (18) to the corresponding QBs, as the associated eigenvalue equations are similar to these equations. For the BIM the eigenvalues k_n and eigenfunctions are determined by solving a quantization condition of the form $\det \hat{A}(k_n) = 0$, where the matrix \hat{A} is obtained from a boundary-integral equation deduced from the Green theorem [14, 17, 18]. In the examples presented in the following we chose for the QB and NB the same dimension 500×500 for \hat{A} , which corresponds to the discretization of the boundary into 500 pieces, and computed it for 600000 values of k in the range of $k \in [0, 100]$ to obtain complete sequences of ≈ 3000 eigenvalues. For the CMM Eq. (16) we considered 5000

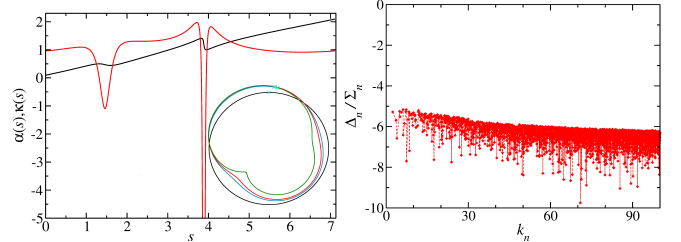


FIG. 1. Left: The angle $\alpha(s)$ of the normal vector with respect to the x axis (black) and boundary curvature (red) for the shape of the Africa billiard defined in Eq. (35) with $\alpha = 0.2$, where s denotes the arclength parameter. The shapes considered in this work are shown in the inset for $\alpha = 0$ (black), $\alpha = 0.1$ (blue), $\alpha = 0.125$ (red) and $\alpha = 0.2$ (green). The crosses mark the zero point of the arclength parameter s , which increases along the boundary in clockwise direction. Right: Relative differences $\Delta_n/\Sigma_n = 2^{\frac{|k_n^{BIM} - k_n^{CMM}|}{k_n^{BIM} + k_n^{CMM}}}$ for the Africa QB with $\alpha = 0.2$. Here, k_n^{BIM} and k_n^{CMM} denote the eigenvalues obtained with the BIM and CMM, respectively.

eigenstates of the circular QB, yielding $\simeq 2500$ reliable eigenvalues, as demonstrated in Fig. 1. There we show the relative deviations of the eigenvalues resulting from the BIM and from the CMM, respectively.

For the NB we used the first 10000 eigenstates of the circular NB to compute the solutions of Eq. (29), Eq. (30) and Eq. (31). The number of eigenstates obtained from the CMM is of the same order as for

the QB, even though we considered there only half the number of eigenstates of the circular QB. Beyond that value, the Weyl formula for NBs [14], which gives the average of the number of eigenvalues $N(k_n)$ below $k = k_n$, $N^{Weyl}(k_n) = \frac{\mathcal{A}}{4\pi} k_n^2 + C$ with \mathcal{A} and C denoting the area of the corresponding NB and a positive constant $C \lesssim 0.5$, is no longer applicable [cf. the left part of Fig. 2]. In fact, to verify whether the eigenvalues obtained from the CMM are those of NBs, we fit a polynomial of the form $N^{smooth}(k_n) = \frac{\tilde{\mathcal{A}}}{4\pi} k_n^2 - \frac{\tilde{\mathcal{L}}}{4\pi} k_n + C$ to $N(k_n)$, which actually is the Weyl formula for non-relativistic QBs with area $\tilde{\mathcal{A}}$ and perimeter $\tilde{\mathcal{L}}$. For the BIM the boundary term $\frac{\tilde{\mathcal{L}}}{4\pi}$ is by a factor of $10^{-5} - 10^{-4}$ smaller than the area term, whereas for the solutions of Eqs. (30) and (31) the factor increases from $\approx 10^{-3}$ to $\approx 10^{-2}$ with increasing deformation of the shape from that of a circle, and for the solutions of Eq. (29) this factor is about 10 times smaller than these values. Accordingly, for the CMM the parameter $\tilde{\mathcal{A}}$ deviates from the expected value, \mathcal{A} .

In the lower panels of the right part of Fig. 2 we show the relative deviations of the eigenvalues obtained with the BIM from those computed with Eq. (31), in the upper panels those between the eigenvalues obtained from Eqs. (29) and (30), respectively. The distances are of similar size for all cases and by at least two decades larger than for the nonrelativistic case, thus confirming that the CMM does not yield solutions of the Dirac equation for NBs. Still, the agreement with the eigenvalues obtained from the exact quantization procedure, i.e., the BIM is good, especially for the solutions of Eq. (29), even for the case with $\alpha = 0.2$. This maybe explained by the fact that the boundary curvature is close to that of the circle except in the region around the bulges. However, generally, as demonstrated in Fig. 2, the deviations between the eigenvalues obtained with the BIM and CMM increase with the deformation of the circular NB, thus corroborating the proof.

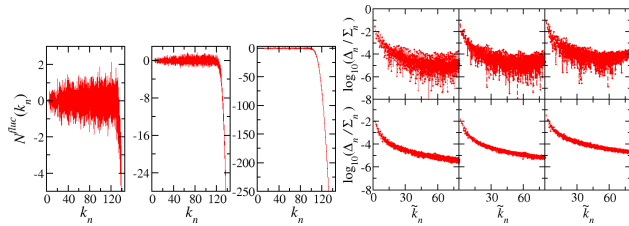


FIG. 2. Left: Difference $N^{fluc}(k_n) = N(k_n) - N^{Weyl}(k_n)$ between the number of eigenvalues $N(k_n)$ of Eq. (31) below $k = k_n$ and the Weyl formula $N^{Weyl}(k_n) = \frac{\mathcal{A}}{4\pi} k_n^2 + C$ for an NB with shape Eq. (35) with $\alpha = 0.1$ (left), $\alpha = 0.125$ (middle) and $\alpha = 0.2$ (right). Right: Relative differences $\Delta_n/\Sigma_n = 2^{\frac{|k_n^a - k_n^b|}{k_n^a + k_n^b}}$ for $\alpha = 0.1$ (left), $\alpha = 0.125$ (middle) and $\alpha = 0.2$ (right). In the upper panels the k_n^a are obtained from Eq. (29) and the k_n^b are deduced from (30), in the lower ones the k_n^a were computed with the BIM and the k_n^b are obtained from Eq. (31).

Furthermore, the boundary wave functions for the BIM

and CMM cases, show clear differences. In Fig. S1 of Sec. A the outgoing flux is shown for two examples. It is of the order of 10^{-16} for the BIM results and agrees well with the analytical result Eq. (34) for the CMM ones. A clear discrepancy is visible for all cases also in the corresponding wave functions shown in Fig. S2 of Sec. A, one reason being that their phases differ due to the differing boundary conditions. The wave functions for state 2508 are scarred along a straight line corresponding to a remnant of the diameter orbit in the original circular NB. It bounces back and forth between two nearly circular focusing boundary segments, and thus is expected to occur in both cases, with dominant support in the region where the boundary curvature is close to unity. Indeed, such scarred wave functions are also observed in the Africa QB. Nevertheless, to get for the CMM case the correct phase along that orbit, the wave function has to be multiplied with a factor in order to fulfill the BC for the NB [cf. Eq. (33)].

A. Example of a billiard for which for the CMM yields solutions that clearly deviate from those of the BIM

We also considered two billiards with shapes given by Eq. (6) with $c_1 = 1$, $c_2 = c_4 = c_5 = 0.1$, and $c_3 = 0.1 -$ exhibiting a mirror symmetry –, respectively, $c_3 = 0.1e^{i\pi/3}$ – deviating along most parts of the boundary from that of a circle. The shapes are shown in the left and right inset of the left part of Fig. 3, respectively. To obtain the solutions of Eqs. (29), (30) and (31) we used the same number of eigenvalues of the corresponding circular QB and NB as in the previous examples. However, in that case only about 1000 eigenvalues could be obtained that comply with the Weyl formula in the sense that the smooth part of the integrated spectral density is well described by that for nonrelativistic QBs, that is, a second-order polynomial [cf. left part of Fig. 3]. Namely $\tilde{\mathcal{L}}$ is by a factor 10^{-5} smaller than the area term for the BIM, whereas for the solutions of Eqs. (30) and (31) this factor is $\approx 10^{-2}$ and $\approx 10^{-1}$ for complex and real c_3 , respectively, and for the solutions of Eq. (29) about 10 times smaller than these values.

It can be seen in Fig. 4 that the solutions of Eqs. (29) and (30) clearly deviate from each other for the shapes with real (blue) and complex (red) c_3 , thus demonstrating that the assumption that the eigenvalues of the NB can be obtained from the sum of Eqs. (29) and (30) with $\mathbf{a} = \mathbf{b}$ is wrong. Also the solutions of Eq. (31) deviate from those obtained with the BIM for the corresponding NB, as exhibited in the right part of Fig. 3 (red). The high accuracy of the eigenvalues computed with the BIM can be deduced from the fact, that $\tilde{\mathcal{A}} = \mathcal{A} + o(10^{-6})$ and $\tilde{\mathcal{L}} \sim 10^{-6}$. Furthermore, to get an estimate for the size of deviations we also show the differences between the eigenvalues $k_n^a = \tilde{k}_n$ of the QB with complex c_3 , computed with the BIM and the CMM Eq. (17) (maroon). These

are a factor 10^{-3} smaller than for the NB. The spectral properties are close to GUE for the eigenvalues of the billiard with complex c_3 , whereas they are close to the GOE for the shape with real c_3 . This is expected, because for that case the shape has a mirror symmetry. However, in contrast to the non-relativistic QB, the associated spinor eigenstates cannot be separated according to their mirror symmetry, so the BIM and also the CMM should be applied to the whole billiard system. Yet, the spectral properties of the eigenvalues obtained from Eqs. (31) and the BIM clearly deviate from each other, when considering for the former more than about 900 eigenvalues. This is illustrated in the right part of Fig. 3 for the shapes with real (blue) and complex (black) c_3 and for the Africa shape with $\alpha = 0.2$. Shown are results for the number variance $\Sigma^2(L)$ in an interval of length L [43] for the NB (open symbols) and the eigenvalues of Eq. (31). As outlined above, these were unfolded with the Weyl formula for QBs (filled symbols), where the number of eigenvalues was chosen as large as possible, that is, such that the fluctuating part of the integrated spectral density fluctuates about zero, implying that there are no missing levels according to the unfolding procedure (open symbols).

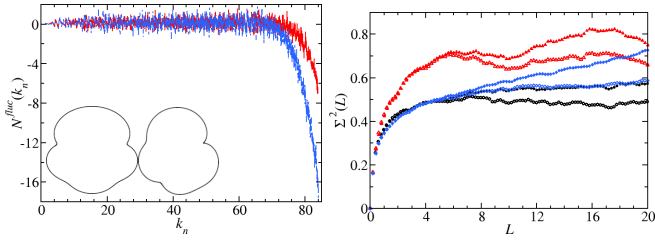


FIG. 3. Left: Difference $N^{fluc}(k_n) = N(k_n) - N^{smooth}(k_n)$ between the number of eigenvalues obtained from Eq. (31), $N(k_n)$, below $k = k_n$ and the best fitting Weyl formula for QBs, $N^{smooth}(k_n) = \frac{\tilde{A}}{4\pi}k_n^2 - \frac{\tilde{C}}{4\pi}k_n + C$ for the shape with real (red) and complex (blue) c_3 [cf. insets]. Right: Comparison of the number variance $\Sigma^2(L)$ computed for the eigenvalues of the NB using BIM (open symbols) and obtained from Eq. (31) for the billiards with real (red) and complex (black) c_3 and for the Africa shape with $\alpha = 0.2$ (blue), respectively. Here, the eigenvalues were unfolded with the Weyl formula for non-relativistic QBs (full symbols), taking into account as many eigenvalues as possible, that is, ensuring that none are missing according to the unfolding procedure.

V. CONCLUSIONS

In [28] and subsequent works of these authors, the CMM is applied to NBs whose shapes originate from a

conformal mapping of a circular shape. Starting point is an ansatz for the spinor components in terms of those of the eigenfunctions of the associated circular NB. These fulfill by construction the BC of that circular NB, but not that of the NB itself. Here, the expansion coefficients in the ansatz for the first spinor component are

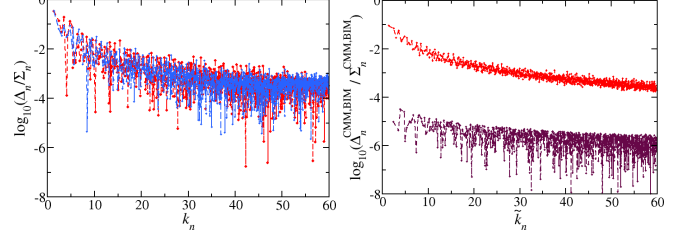


FIG. 4. Left: Relative differences $\Delta_n / \Sigma_n = 2^{\frac{|k_n^a - k_n^b|}{k_n^a + k_n^b}}$ between the eigenvalues k_n^a obtained from Eq. (29) and k_n^b from Eq. (30) for the billiard with real c_3 (blue, left inset of Fig. 3) and complex c_3 (red, right inset of Fig. 3). Right: same as left for the eigenvalues k_n^a of the shape Eq. (6) with complex c_3 computed with the BIM and k_n^b obtained with Eq. (31) (red), and for the corresponding QB with eigenvalues $k_n^a = k_n$ computed with the BIM and k_n^b obtained from Eq. (17) (maroon).

set equal to those of the second one, thereby ignoring their relation through the associated Dirac equation, and the Schrödinger equation Eq. (11) is solved for their sum, Eq. (31). We demonstrate in this work – in the Secs. IV and IV A also numerically – that equations (29), (30) for the spinor components and Eq. (31) do not have common solutions. Accordingly, the solutions of Eq. (31) are none of the Dirac equation for NBs and it is questionable to what extent they are connected to those of relativistic QBs. This discrepancy originates from the fact, that the conditional equation deduced from the BC Eq. (5) for the circular NB differs from that for non-circular ones. Thus, the assumption, that the matrices entering the generalized eigenvalue problem Eq. (29) are independent of k , is not applicable. On the contrary, for non-relativistic QBs the BC is independent of φ and fulfilled for each term in the CMM expansion of the eigenstates in terms of those of the nonrelativistic circular QB [cf. Eq. (16)].

VI. ACKNOWLEDGEMENT

The author acknowledges financial support from the Institute for Basic Science in Korea through the project IBS-R024-D1.

[1] Y. G. Sinai, Dynamical systems with elastic reflections, Russ. Math. Surv. **25**, 137 (1970).

[2] L. A. Bunimovich, On the ergodic properties of nowhere dispersing billiards, Commun. Math. Phys. **65**, 295

(1979).

[3] M. V. Berry, Regularity and chaos in classical mechanics, illustrated by three deformations of a circular 'billiard', *Eur. J. Phys.* **2**, 91 (1981).

[4] M. Giannoni, A. Voros, and J. Zinn-Justin, eds., *Chaos and Quantum Physics* (Elsevier, Amsterdam, 1989).

[5] H.-J. Stöckmann and J. Stein, "quantum" chaos in billiards studied by microwave absorption, *Phys. Rev. Lett.* **64**, 2215 (1990).

[6] A. Richter, Playing billiards with microwaves - quantum manifestations of classical chaos, in *Emerging Applications of Number Theory*, The IMA Volumes in Mathematics and its Applications, Vol. 109, edited by D. A. Hejhal, J. Friedman, M. C. Gutzwiller, and A. M. Odlyzko (Springer, New York, 1999) p. 479.

[7] F. Haake, S. Gnutzmann, and M. Kuś, *Quantum Signatures of Chaos* (Springer-Verlag, Heidelberg, 2018).

[8] S. Sridhar, Experimental observation of scarred eigenfunctions of chaotic microwave cavities, *Phys. Rev. Lett.* **67**, 785 (1991).

[9] H.-D. Gräf, H. L. Harney, H. Lengeler, C. H. Lewenkopf, C. Rangacharyulu, A. Richter, P. Schardt, and H. A. Weidenmüller, Distribution of eigenmodes in a superconducting stadium billiard with chaotic dynamics, *Phys. Rev. Lett.* **69**, 1296 (1992).

[10] J. Stein and H.-J. Stöckmann, Experimental determination of billiard wave functions, *Phys. Rev. Lett.* **68**, 2867 (1992).

[11] P. So, S. M. Anlage, E. Ott, and R. Oerter, Wave chaos experiments with and without time reversal symmetry: GUE and GOE statistics, *Phys. Rev. Lett.* **74**, 2662 (1995).

[12] S. Deus, P. M. Koch, and L. Sirk, Statistical properties of the eigenfrequency distribution of three-dimensional microwave cavities, *Phys. Rev. E* **52**, 1146 (1995).

[13] B. Dietz and A. Richter, Quantum and wave dynamical chaos in superconducting microwave billiards, *Chaos* **25**, 097601 (2015).

[14] M. V. Berry and R. J. Mondragon, Neutrino billiards: Time-reversal symmetry-breaking without magnetic fields, *Proc. R. Soc. London A* **412**, 53 (1987).

[15] V. Heuveline, On the computation of a very large number of eigenvalues for selfadjoint elliptic operators by means of multigrid methods, *J. Comput. Phys.* **184**, 321 (2003).

[16] E. Vergini and M. Saraceno, Calculation by scaling of highly excited states of billiards, *Phys. Rev. E* **52**, 2204 (1995).

[17] A. Bäcker, Numerical Aspects of Eigenvalue and Eigenfunction Computations for Chaotic Quantum Systems, in *The Mathematical Aspects of Quantum Maps*, edited by M. D. Esposti and S. Graffi (Springer Berlin Heidelberg, Berlin, Heidelberg, 2003) pp. 91–144.

[18] B. Dietz and Z.-Y. Li, Semiclassical quantization of neutrino billiards, *Phys. Rev. E* **102**, 042214 (2020).

[19] B. Dietz and A. Richter, Intermediate statistics in singular quarter-ellipse shaped microwave billiards*, *J. Phys. A: Math. Theor.* **55**, 314001 (2022).

[20] J. Wiersig, Boundary element method for resonances in dielectric microcavities, *J. Opt. A: Pure Appl. Opt.* **5**, 53 (2002).

[21] R. Ketzmerick, F. Lorenz, and J. R. Schmidt, Semiclassical limit of resonance states in chaotic scattering, *Phys. Rev. Lett.* **134**, 020404 (2025).

[22] C.-H. Yi, B. Dietz, J.-H. Han, and J.-W. Ryu, Decay rates of optical modes unveiling the island structures in mixed phase space, *Phys. Rev. A* **111**, 033509 (2025).

[23] Y. Okada, A. Shudo, S. Tasaki, and T. Harayama, On the boundary element method for billiards with corners, *J. Phys. A: Math. Gen.* **38**, 6675 (2005).

[24] G. Veble, T. Prosen, and M. Robnik, Expanded boundary integral method and chaotic time-reversal doublets in quantum billiards, *New J. Phys.* **9**, 15 (2007).

[25] P. Yu, B. Dietz, and L. Huang, Quantizing neutrino billiards: an expanded boundary integral method, *New J. Phys.* **21**, 073039 (2019).

[26] B. Dietz, Semi-Poisson statistics in relativistic quantum billiards with shapes of rectangles, *Entropy* **25**, 10.3390/e25050762 (2023).

[27] M. Robnik, Quantising a generic family of billiards with analytic boundaries, *J. Phys. A: Math. Gen.* **17**, 1049 (1984).

[28] H. Xu, L. Huang, Y.-C. Lai, and C. Grebogi, Chiral scars in chaotic dirac fermion systems, *Phys. Rev. Lett.* **110**, 064102 (2013).

[29] L. Huang, H.-Y. Xu, C. Grebogi, and Y.-C. Lai, Relativistic quantum chaos, *Phys. Rep.* **753**, 1 (2018).

[30] M.-Y. Song, Z.-Y. Li, H.-Y. Xu, L. Huang, and Y.-C. Lai, Quantization of massive Dirac billiards and unification of nonrelativistic and relativistic chiral quantum scars, *Phys. Rev. Research* **1**, 033008 (2019).

[31] Z.-Y. Li, L.-L. Ye, R.-H. Ni, C.-Z. Wang, L. Huang, Y.-C. Lai, and C. Grebogi, Relativistic quantum scarring, spin-induced phase, and quantization in a symmetric dirac billiard system, *J. Phys. A: Math. Theor.* **55**, 374003 (2022).

[32] H. Weyl, Elektron und Gravitation. I, *Z. Physik* **56**, 330 (1929).

[33] This choice of BCs is not the only one guaranteeing self-adjointness of the Dirac Hamiltonian and zero outgoing current [44, 45].

[34] B. Dietz and U. Smilansky, A scattering approach to the quantization of billiards—the inside–outside duality, *Chaos* **3**, 581 (1993).

[35] M. V. Berry and M. Robnik, Statistics of energy levels without time-reversal symmetry: Aharonov-Bohm chaotic billiards, *J. Phys. A* **19**, 649 (1986).

[36] M. C. Gutzwiller, Periodic orbits and classical quantization conditions, *J. Math. Phys.* **12**, 343 (1971).

[37] J. Bolte and S. Keppeler, A semiclassical approach to the Dirac equation, *Ann. Phys.* **274**, 125 (1999).

[38] J. Wurm, A. Rycerz, İ. Adagideli, M. Wimmer, K. Richter, and H. U. Baranger, Symmetry classes in graphene quantum dots: Universal spectral statistics, weak localization, and conductance fluctuations, *Phys. Rev. Lett.* **102**, 056806 (2009).

[39] R. Balian and B. Duplantier, Electromagnetic waves near perfect conductors. I. Multiple scattering expansions. Distribution of modes, *Ann. Phys. (N.Y.)* **104**, 300 (1977).

[40] C. Dembowski, B. Dietz, H.-D. Gräf, A. Heine, T. Papenbrock, A. Richter, and C. Richter, Experimental test of a trace formula for a chaotic three-dimensional microwave cavity, *Phys. Rev. Lett.* **89**, 064101 (2002).

[41] B. Dietz, Circular and elliptical neutrino billiards: A semiclassical approach, *Act. Phys. Pol. A* **136**, 770 (2019).

[42] B. Dietz, Unidirectionality and Husimi functions in constant-width neutrino billiards, *J. Phys. A: Math. Theor.* **55**, 474003 (2022).

[43] M. L. Mehta, *Random Matrices* (Elsevier, Amsterdam, 2004).

[44] W. A. Gaddah, Exact solutions to the Dirac equation for equilateral triangular billiard systems, *J. Phys. A: Math. Theor.* **51**, 385304 (2018).

[45] W. Greiner and A. Schäfer, eds., *Quantum Chromodynamics* (Springer, New York, 1994).

Appendix A: Appendix

1. Some technical details

The plane-wave expansion for the second component Eq. (14) in the main text is obtained by inserting the ansatz for the first component, Eq. (13) into Eq. (9) and employing the equalities

$$\frac{1}{z^*[w'(z)]^*} \left(r \frac{\partial}{\partial r} + i \frac{\partial}{\partial \varphi} \right) |w(z)| = e^{i\theta(z)}, \quad (\text{A1})$$

$$\begin{aligned} \frac{1}{z^*[w'(z)]^*} \left(r \frac{\partial}{\partial r} + i \frac{\partial}{\partial \varphi} \right) e^{il\theta(z)} &= -\frac{l}{|w(z)|} e^{i(l+1)\theta(z)}, \\ \frac{1}{zw'(z)} \left(r \frac{\partial}{\partial r} - i \frac{\partial}{\partial \varphi} \right) e^{il\theta(z)} &= \frac{l}{|w(z)|} e^{i(l-1)\theta(z)}, \end{aligned} \quad (\text{A2})$$

and

$$J_{l-1}(x) = \frac{l}{x} J_l(x) + \frac{dJ_l(x)}{dx}, \quad J_{l+1}(x) = \frac{l}{x} J_l(x) - \frac{dJ_l(x)}{dx}. \quad (\text{A3})$$

The spinor eigenfunction,

$$\Phi_{n,\nu}(r, \varphi) = \begin{pmatrix} \Phi_{1n,\nu}(r, \varphi) \\ \Phi_{2n,\nu}(r, \varphi) \end{pmatrix}, \quad (\text{A4})$$

are orthogonal to each other,

$$\int_0^{r_0} r dr \int_0^{2\pi} d\varphi \Phi_{m,\mu}(r, \varphi) \cdot \Phi_{n,\nu}(r, \varphi) \quad (\text{A5})$$

$$= \delta_{n,m} 2\pi \int_0^{r_0} r dr [J_{m,\mu}(\kappa_{m,\mu} r) J_{m,\nu}(\kappa_{m,\nu} r) + J_{m+1,\mu}(\kappa_{m,\mu} r) J_{m+1,\nu}(\kappa_{m,\nu} r)] \mathcal{N}_{m,\mu} \mathcal{N}_{m,\nu} \quad (\text{A6})$$

$$\propto \delta_{n,m} \delta_{\nu,\mu}. \quad (\text{A7})$$

Namely, for $\Phi_{1n,\nu}(r, \varphi)$ we have

$$\begin{aligned} &\int_0^{r_0} r dr \int_0^{2\pi} d\varphi J_n(\kappa_{n,\nu} r) J_m(\kappa_{m,\mu} r) e^{i(n-m)\varphi}, \\ &= 2\pi \delta_{n,m} \frac{\kappa_{m,\nu} r_0 J_{m+1}(\kappa_{m,\nu} r_0) J_m(\kappa_{m,\mu} r_0) - \kappa_{m,\mu} r_0 J_{m+1}(\kappa_{m,\mu} r_0) J_m(\kappa_{m,\nu} r_0)}{\kappa_{m,\nu}^2 - \kappa_{m,\mu}^2}, \\ &= 2\pi \delta_{n,m} \begin{cases} \frac{J_m(\kappa_{m,\nu} r_0) J_m(\kappa_{m,\mu} r_0)}{\kappa_{m,\nu} + \kappa_{m,\mu}}, & \nu \neq \mu \\ -r_0^2 J_m(\kappa_{m,\mu} r_0) J'_{m,\mu}(\kappa_{m,\mu} r_0), & \nu = \mu \end{cases}, \end{aligned} \quad (\text{A8})$$

and similarly for $\Phi_{2n,\nu}(r, \varphi)$

$$\begin{aligned} &\int_0^{r_0} r dr \int_0^{2\pi} d\varphi J_{n+1}(\kappa_{n,\nu} r) J_{m+1}(\kappa_{m,\mu} r) e^{i(n-m)\varphi}, \\ &= 2\pi \delta_{n,m} \frac{\kappa_{m,\mu} r_0 J_m(\kappa_{m,\mu} r_0) J_{m+1}(\kappa_{m,\nu} r_0) - \kappa_{m,\nu} r_0 J_m(\kappa_{m,\nu} r_0) J_{m+1}(\kappa_{m,\mu} r_0)}{\kappa_{m,\nu}^2 - \kappa_{m,\mu}^2}, \\ &= 2\pi \delta_{n,m} \begin{cases} \frac{-J_m(\kappa_{m,\nu} r_0) J_m(\kappa_{m,\mu} r_0)}{\kappa_{m,\nu} + \kappa_{m,\mu}}, & \nu \neq \mu \\ r_0^2 J_m(\kappa_{m,\mu} r_0) J'_{(m+1),\mu}(\kappa_{m,\mu} r_0), & \nu = \mu \end{cases}, \end{aligned} \quad (\text{A9})$$

where we employed the BC Eq. (20) in the main text, implying that for $\nu \neq \mu$ the sum of the contributions from the two spinor components cancel each other and

$$\frac{1}{\mathcal{N}_{m,\mu}\mathcal{N}_{n,\nu}} \int_0^{r_0} r dr \int_0^{2\pi} d\varphi \Phi_{m,\mu}(r, \varphi) \cdot \Phi_{n,\nu}(r, \varphi) = \delta_{n,m} \delta_{\nu,\mu} \pi r_0^2 \left[\frac{dJ_{(m+1),\mu}^2(x)}{dx} - \frac{dJ_{m,\mu}^2(x)}{dx} \right] \Big|_{(x=\kappa_{m,\mu})} = \frac{1}{\mathcal{N}_{n,\nu}^2}. \quad (\text{A10})$$

In analogy to the nonrelativistic case, Eq. (19) in the main text, the matrices $\hat{\mathcal{K}}_1$, $\hat{\mathcal{K}}_2$, $\hat{\mathcal{J}}_1$ and $\hat{\mathcal{J}}_2$, are defined as

$$\begin{aligned} \hat{\mathcal{K}}_{1,jj'} &= 2\pi \delta_{nm} \mathcal{N}_{n,\nu} \mathcal{N}_{m,\mu} \int_0^{r_0} r dr J_m(\kappa_{m,\mu} r) J_m(\kappa_{m,\nu} r) \kappa_{m,\nu}^2, \\ \hat{\mathcal{K}}_{2,jj'} &= 2\pi \delta_{nm} \mathcal{N}_{n,\nu} \mathcal{N}_{m,\mu} \int_0^{r_0} r dr J_{m+1}(\kappa_{m,\mu} r) J_{m+1}(\kappa_{m,\nu} r) \kappa_{m,\nu}^2, \\ \hat{\mathcal{J}}_{i1,jj'} &= \mathcal{N}_{n,\nu} \mathcal{N}_{m,\mu} \int_0^{r_0} r dr \int_0^{2\pi} d\varphi |w'(z)|^2 J_m(\kappa_{m,\mu} r) J_n(\kappa_{n,\nu} r) i^{(n-m)} e^{i(n-m)\varphi}, \\ \hat{\mathcal{J}}_{2,jj'} &= \mathcal{N}_{n,\nu} \mathcal{N}_{m,\mu} \int_0^{r_0} r dr \int_0^{2\pi} d\varphi |w'(z)|^2 J_{m+1}(\kappa_{m,\mu} r) J_{n+1}(\kappa_{n,\nu} r) i^{(n-m)} e^{i(n-m)\varphi}, \end{aligned} \quad (\text{A11})$$

with $[m, \mu] = [l(j), \lambda(j)]$, $[n, \nu] = [l(j'), \lambda(j')]$.

2. Comparison of wave functions obtained from CMM and BIM for the Africa billiard with shape given in Eq. (E1) with $\alpha = 0.2$

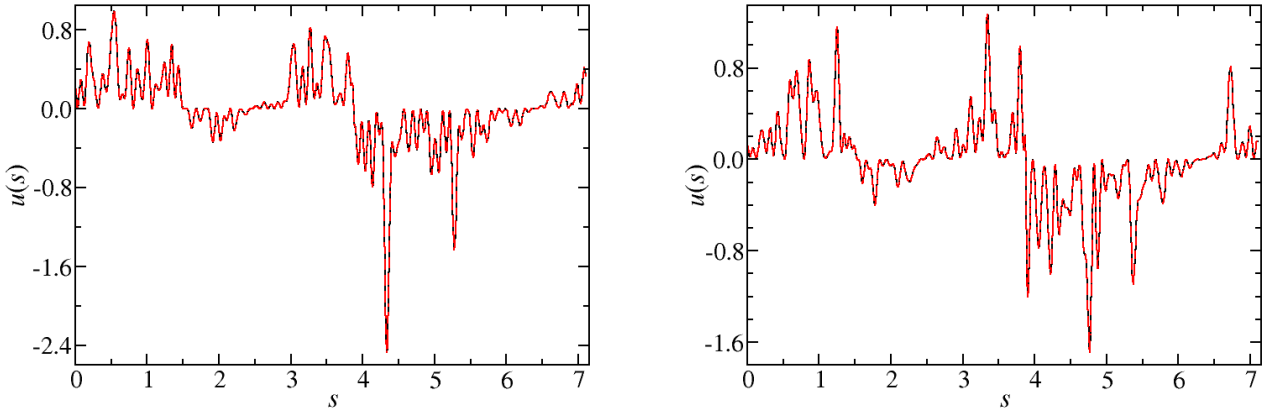


FIG. A1. Outgoing flux along the boundary for the eigenstates 2507 (left) and 2508 (right) computed with CMM (black). Agreement with the analytical result Eq. (34) (red) of the main text is excellent.

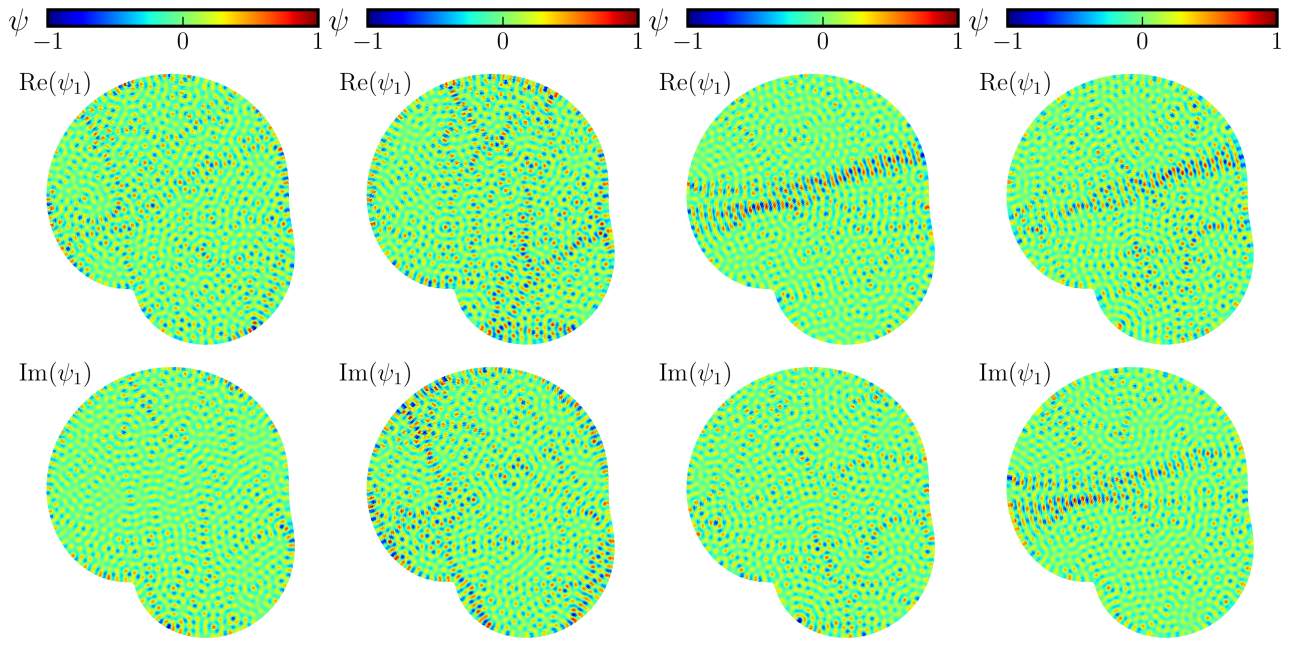


FIG. A2. Real and Imaginary parts of the first spinor component obtained from the BIM (1st and 3rd column) and CMM (2nd and 4th column) for the eigenstate 2507 (left pair of columns) and 2508 (right pair of column).